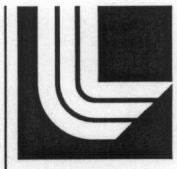

LAWRENCE
LIVERMORE
NATIONAL
LABORATORY

UCRL-JC-155218

Measurement of the Ansolute Hohlraum Wall Albedo Under Ignition Foot Drive Conditions

O.S. Jones, S.H. Glenzer, L.J. Suter, R.E. Turner, K.M. Campbell, E.L. Dewald, B.A. Hammel, R.L. Kauffman, O.L. Landen, M.D. Roden, R.J. Wallace, F.A. Weber

August 26, 2003

3rd IFSA Conference, Monterey, CA, September 7-12, 2003

This work was performed under the auspices of the U.S. Department of Energy by University of California, Lawrence Livermore National Laboratory under Contract W-7405-Eng-48.

Measurement of the absolute hohlraum wall albedo under ignition foot drive conditions

O. S. Jones, S. H. Glenzer, L. J. Suter, R. E. Turner, K. M. Campbell, E. L. Dewald, B. A. Hammel, R. L. Kauffman, O. L. Landen, M. D. Rosen, R. J. Wallace, F. A. Weber

Lawrence Livermore National Laboratory, Livermore, California 94551

Abstract

We present the first measurements of the absolute albedos of hohlraums made from gold or from high-Z mixtures. The measurements are performed over the range of radiation temperatures (70-100 eV) expected during the foot of an indirect-drive temporally-shaped ignition laser pulse, where accurate knowledge of the wall albedo (i.e. soft x-ray wall re-emission) is most critical for determining capsule radiation symmetry. We find that the gold albedo agrees well with calculations using the super transition array opacity model, potentially providing additional margin for ICF ignition.

Indirect drive inertial confinement fusion (ICF) uses high intensity lasers or particle beams to heat a high-Z cavity, or hohlraum, that produces soft x-rays that are characterized by a radiation temperature, T_{RAD} [1]. The x-rays heat and ablate the surface of a DT-filled fusion capsule, compressing and heating the DT fuel until it ignites. Current indirect drive target designs predict that ignition and gain can be achieved by heating hohlraums with a temporally-shaped 1.5-2 MJ, 0.35-micron laser pulse [2-5]. The baseline ignition laser pulse creates a time-dependent radiation drive that consists of a 10-ns long "foot" at 80-100 eV, followed by a rapid increase in the drive temperature to a peak of 300 eV at 15 ns. The hohlraum conditions during the long foot of the pulse, including the uniformity of the radiation flux, are important. The level of the foot's drive sets the strength of the first shock, while any spatial illumination non-uniformities during the foot lead to asymmetric drive.

The albedo is the ratio of the re-emitted x-ray flux to the incident x-ray flux. Accurate knowledge of this quantity is important to the ignition effort because it affects our estimates of the asymmetry during the foot. Radiation uniformity depends on a variety of parameters including the location of the laser spots on the hohlraum wall and the x-ray brightness of those spots relative to the soft x-ray re-emission from the unirradiated wall. Higher albedo leads to a larger ratio of wall re-emission to spot brightness, which reduces capsule asymmetries due to laser power imbalance and beam mispointing.

In this letter, we report on the first experiments that measure the absolute albedo of hohlraums made from several different high-Z materials at radiation temperatures close to the NIF foot radiation temperature. We use a novel experimental technique in which the high-Z hohlraum from which we infer the albedo is heated by soft x-rays and not by a laser, thus eliminating x-ray conversion efficiency and laser backscatter as parameters in the data analysis [6]. Moreover, the same instrument measures the flux incident upon the high-Z hohlraum wall and the flux re-emitted from the wall. This technique results in a measurement error in the albedo of only +/- 0.05. We show that the albedo of gold inferred from the experiment matches well with predictions using the radiation hydrodynamics code, LASNEX [7], with opacities from the super transition array (STA) model [8,9]. The measured albedo is larger than predicted from calculations that use the average-atom XSN model [10] for the opacity. This is important because the original NIF laser uniformity specifications [11] were based on modeling of gold hohlraums that used the average-atom XSN approximation for the opacities, resulting in an albedo at the end of the 80 eV foot pulse

that is ~15% lower than predicted using STA opacities. A simplified hohlraum model [1] shows that having a 15% larger albedo in the foot than predicted by XSN results in approximately 1.7 times more attenuation of the radiation asymmetry due to random variations in laser power or pointing during the foot due to the increased wall re-emission relative to the laser spot brightness. This new finding means the radiation on the capsule should be more uniform than previously estimated, providing additional margin for ignition.

The experiments were performed at the Omega laser facility. The experimental setup is shown in Figure 1. The basic configuration (Fig. 1b) consisted of two attached hohlraums. The primary hohlraum (1600 μm diameter, 1125 μm length) produced the soft x-ray drive that heated the secondary hohlraum, whose wall re-emission was measured in order to infer the wall albedo. The primary hohlraum was heated on one side by 15 laser beams that delivered 6.5 kJ in a 1.5-ns temporally-flat pulse. It reached a peak radiation temperature of ~160 eV and that radiation heated the larger secondary hohlraum. The size and materials of the attached secondary hohlraums were varied. We tested secondary hohlraums (with 3440 μm diameter, and 3750 μm length) made of gold, uranium (alloyed with 14% atomic fraction niobium), and a mixture (or "cocktail") [12-14] made up of 52% uranium, 8% niobium, 20% gold, and 20% dysprosium. These secondary hohlraums reached a peak radiation temperature of ~100 eV. We also tested a larger gold secondary hohlraum (with 4400 μm diameter, and 4800 μm length), which had a lower peak radiation temperature (~70 eV) than the smaller secondary hohlraums. All secondary hohlraums had a 1000 μm diameter diagnostic hole on the end.

The radiation power out of the secondary hohlraum diagnostic hole (P_d) was measured by the Dante filtered diode array [15] and also by a photoconductive detector (PCD) [16]. To obtain a direct measurement of the power leaving the primary hohlraum and heating the secondary hohlraum (the radiation source power, P_s), we also shot the primary hohlraum without the secondary attached (Fig. 1a), so that the power from the primary (P_s) could be measured with the same two instruments as P_d. Figure 2 shows the time-dependent ratio of the Dante measurements of the radiation power escaping the 3440 μm diameter gold secondary hohlraum diagnostic hole to the radiation power escaping the open end of the primary hohlraum in the associated primary-only shot. We will show that this ratio depends on the albedo of the secondary hohlraum wall. The curves are from LASNEX calculations of the double hohlraum

configuration that use the STA or XSN opacity models. The predicted time-dependent power ratio from the STA opacity model lies within the experimental error bars, whereas the XSN prediction does not.

The secondary hohlraum wall albedo can be related to the Dante measurements of P_s and P_d through a radiation power balance model [17,18]. The radiation power balance for the secondary hohlraum can be formulated as

$$P_s = P_h + P_d + P_w \tag{1}$$

where P_s is the source radiation power coming from the primary hohlraum, and P_h, P_d, and P_w are the radiation sinks leaving the secondary hohlraum through the hole between the two hohlraums, the Dante hole, and into the wall, respectively (see Fig. 1). We define the average radiation temperature in the secondary hohlraum, T_{RAD}, by equating the total frequency-integrated radiation flux inside the hohlraum to a blackbody flux σT_{RAD}^4, where σ is the Stefan-Boltzmann constant. The radiation power leaving the secondary through holes (P_h and P_d) is simply the radiation flux inside the secondary (σT_{RAD}^4) times the hole areas (A_h and A_d). The remaining term, P_w, depends on the fraction of the impinging radiation that is absorbed by the wall (i.e. what is not absorbed is re-emitted and therefore not lost). We define the albedo, α, as the ratio of the emitted radiation flux (F_{out}) to the incident radiation flux (F_{in}). That is, $\alpha = F_{out}/F_{in}$. Since the flux re-emitted by the wall is proportional to α, the radiation power absorbed by the wall is $(1-\alpha)$ times the wall area (A_w). When P_h, P_d, and P_w are expressed in terms of T_{RAD} and α and substituted into equation (1), we find that

$$P_s = \sigma T_{RAD}^4 \left[A_h + A_d + A_w (1-\alpha) \right] \tag{2}$$

The radiation temperature of the secondary hohlraum (T_{RAD}) in equation (2) is inferred from the measured power per steradian from the secondary hohlraum (P_{d2}) by noting that Dante measures the re-emitted flux from the secondary wall, whereas σT_{RAD}^4 in equation (2) is the flux incident on the wall, which is related to the re-emitted flux via the albedo. We can express the re-emitted flux as

$$\alpha \sigma T_{RAD}^4 = \alpha F_{in,avg} = \frac{1}{C_2} \alpha F_{in,view} = \frac{1}{C_2} \frac{P_{d2} \pi}{A_d \sin \beta} \tag{3}$$

where β is the Dante view angle relative to the wall normal (see Fig. 1), $F_{in,avg}$ is the average incident flux over the entire secondary hohlraum wall (A_w), $F_{in,view}$ is the incident flux over the portion of the secondary

hohlraum wall viewed by Dante, and C_2 is the factor that corrects for the nonuniformity of the incident flux. We calculated the spatial variation of the flux using a radiation viewfactor code. This analysis included the effects of the primary hohlraum laser spots and assumed a primary hohlraum albedo of 0.7. Figure 3a shows C_2 as a function of the secondary hohlraum albedo for both sizes of secondary hohlraum.

The total source power (P_s) is related to the power per steradian measured with Dante in the primary-hohlraum shot (P_{d1}) by

$$P_s = C_1 P_{d1} \frac{\pi}{\sin\beta}$$

where C_1 is a factor that accounts for the angle-dependence of the emission due to Dante's viewing a combination of laser spots, unirradiated wall, and laser entrance hole (see Fig. 1). From a Lasnex calculation of the gold primary hohlraum, we find that C_1 varies between 0.85-1.0 during the experiment, as shown in Figure 3b.

Substituting equations (3) and (4) into (2), we get the following equation relating the albedo to the experimentally measured quantities:

$$\alpha C_1 C_2 = \left[1 + \frac{A_h}{A_d} + \frac{A_w}{A_d}(1-\alpha)\right]\frac{P_{d2}}{P_{d1}} \qquad (5)$$

We determined from radiation hydrodynamics calculations of the double hohlraum system that equation (5) is self-consistent to within about 3%, indicating that the radiation power balance model is appropriate for extracting the hohlraum albedo from the experimental measurements, and, conversely, that the ratio of the secondary power to the primary power is related in a simple way to the albedo of the secondary hohlraum.

To estimate experimental uncertainty in our determination of the albedo we use equation (5), neglecting $\left(A_h/A_d + 1\right)$ because it is much smaller than $\left(A_w/A_d\right)(1-\alpha)$ and take the logarithmic derivative to find that $d\alpha \approx \alpha(1-\alpha)dP_R/P_R$, where $P_R = \left(P_{d2}/P_{d1}\right)\left[1/\left(C_1C_2\right)\right]$ We estimate that the error in P_R is approximately +/-20%. This error includes the errors in the model equation, the Dante channel calibrations, and the spectral unfold to get the total Dante power from the channel signals and response functions. The resulting error in the inferred albedo is approximately 0.05 over the range of measured albedos at peak T_{RAD} (0.4-0.6).

Figure 4 summarizes the data from all the experiments at peak T_{RAD} (t = 1.5 ns), and compares it to the results of our LASNEX simulations with the STA opacity models. The measured albedo points are obtained from equation (5) by substituting the measured Dante primary-to-secondary power ratio at 1.5 ns and the hohlraum dimensions. The Lasnex values are obtained by substituting the simulated primary-to-secondary power ratio (at the Dante viewing angle) into equation (5). For the gold and cocktail hohlraums, we see good agreement between the data and the STA prediction. The only material that did not follow the expected trends was uranium, which has a measured albedo that is above the STA prediction. Direct measurements of the uranium opacity in this temperature regime would be beneficial to determining whether STA is correctly predicting the opacity of uranium.

The STA points for gold at 100 eV in Fig. 4 are consistent with the albedo and opacity scalings developed by Rosen [19], who noted that the inaccuracy of the XSN opacity for gold at 70-100 eV is attributable to the lack of n = 4 to 4 transitions near photon energies of 200-300 eV in the XSN average atom approximation. The second Dante channel covers this important spectral range near the Planckian peak, from ~ 200-280 eV. Figure 5 compares the measured and calculated Dante channel 2 signal ratios (secondary to primary) for the 100eV gold secondary hohlraum. The ratio extracted from the STA calculation agrees with the data and is a factor of 2 above the XSN value, providing more experimental verification that STA is needed to accurately model gold at this radiation temperature.

In summary, we have made the first absolute measurements of the albedo of high-Z hohlraums in the temperature range of 70-100 eV, which is the range of temperatures that characterize the foot of an indirect drive ignition pulse. We found that albedo of gold agrees well with LASNEX predictions that use the STA opacity model and lies well above the values predicted using the average atom XSN model for the opacity. The higher STA albedo results in a more uniform radiation flux on the ignition capsule during the foot than previously assumed, providing additional margin for ignition.

References

1. J. Lindl, Inertial Confinement Fusion, Springer-Verlag, New York, 1998
2. S. W. Haan, et al., Phys. Plasmas **2**, 2480 (1995)
3. T. R. Dittrich, et al., Phys. Plasmas **6**, 2164 (1999)
4. D. C. Wilson, et al., Phys. Plasmas **5**, 1953 (1998)
5. W. J. Krauser, et al., Phys. Plasmas **3**, 2084 (1996)
6. S. H. Glenzer, et al., Phys. Rev. Lett. **80**, 2845 (1998)
7. G. B. Zimmerman and W. L. Kruer, Comments Plasma Phys. Controlled Fusion **2**, 51 (1975).
8. A. Bar-Shalom, et al., Phys. Rev. A **40**, 3183 (1989)
9. M. Klapisch, et al., Phys. Plasmas **8**, 1817 (2001)
10. W. A. Lokke and W. H. Grasberger, LLNL Report UCRL-52276 (1977).
11. O. S. Jones, et al., 'The NIF Power Balance," Supplement to Proceedings of SPIE Vol. 3492, 49 (1998).
12. H. Nishimura, et al., Appl. Phys. Lett. **62**, 1344 (1993)
13. T. J. Orzechowski, et al., Phys. Rev. Lett. **77**, 3545 (1996)
14. D. Columbant, M. Klapisch, and A. Bar-Shalom, Phys. Rev. E **57**, 3411 (1998)
15. H. N. Kornblum and R. L. Kauffman, Rev. Sci. Instrum. **57**, 2179 (1986)
16. R. E. Turner, et al., Rev. Sci. Instrum. **70**, 656 (1999)
17. L. Suter, et al., Phys. Plasmas **3**, 2057 (1996)
18. R. L. Kauffmann, et al., Phys. Rev. Lett. **73**, 2320 (1994)
19. M. D. Rosen, Phys. Plasmas **3**, 1803 (1996)

Figures

Fig. 1. Schematic of the (a) primary and (b) double hohlraum experiment together with x-ray power diagnostics and calculated x-ray emission.

Fig. 2. Albedo for a 3440 μm diameter gold secondary hohlraum extracted from measured secondary hohlraum to primary hohlraum radiation power ratio and compared to LASNEX predictions.

Fig. 3 (a) C_2 in equation (5) as a function of the secondary hohlraum albedo. (b) C_{11} in equation (5) as a function of time.

Fig. 4 (a) Comparison of the measured (squares) and predicted (triangles) hohlraum albedos at peak T_{RAD} for different secondary hohlraums. (b) Measured and predicted ratios of the secondary hohlraum Dante channel 2 (200-280 eV) signal to the primary channel 2 signal.

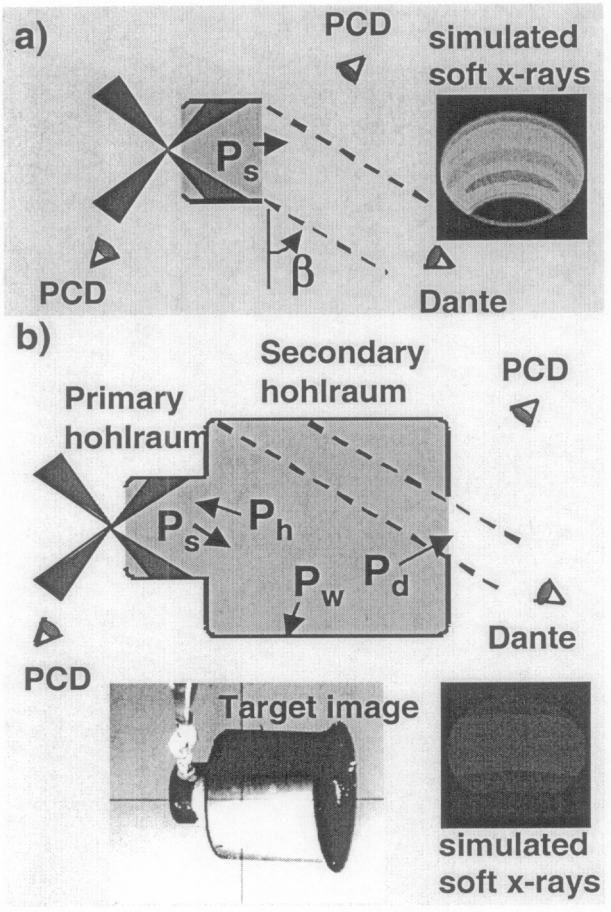
a)
PCD
simulated
soft x-rays
P_s
β
PCD
Dante
b)
Secondary
hohlraum
PCD
Primary
hohlraum
P_s
P_h
P_w
P_d
Dante
PCD
Target image
simulated
soft x-rays

Fig. 1

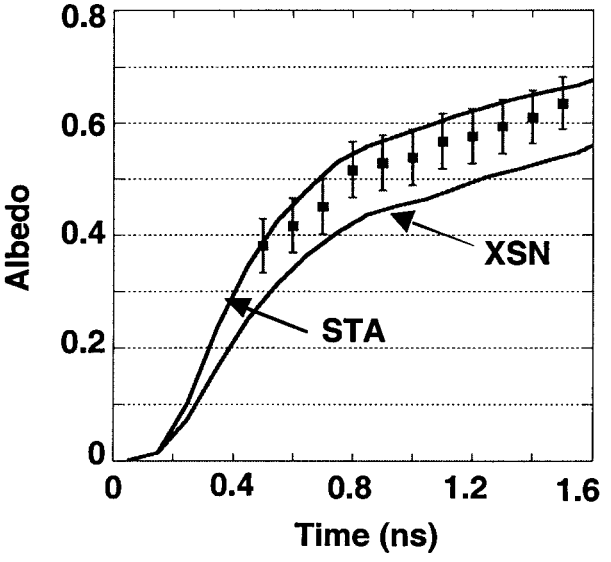

Fig. 2

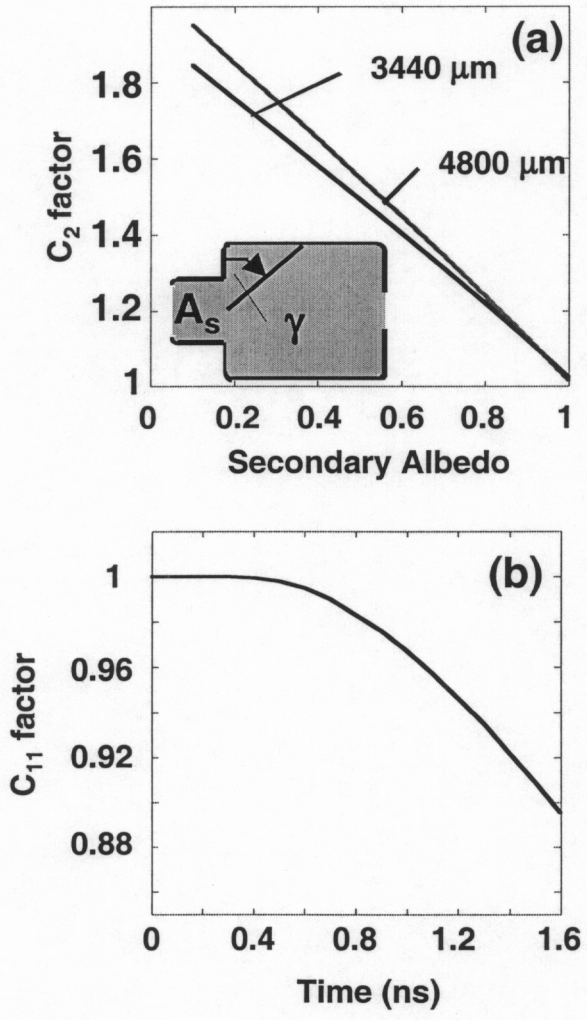
(a)
3440 μm
4800 μm
1.8
1.6
1.4
1.2
1
C_2 factor
A_s
γ
0
0.2
0.4
0.6
0.8
1
Secondary Albedo
(b)
1
0.96
0.92
0.88
C_{11} factor
0
0.4
0.8
1.2
1.6
Time (ns)

Fig. 3

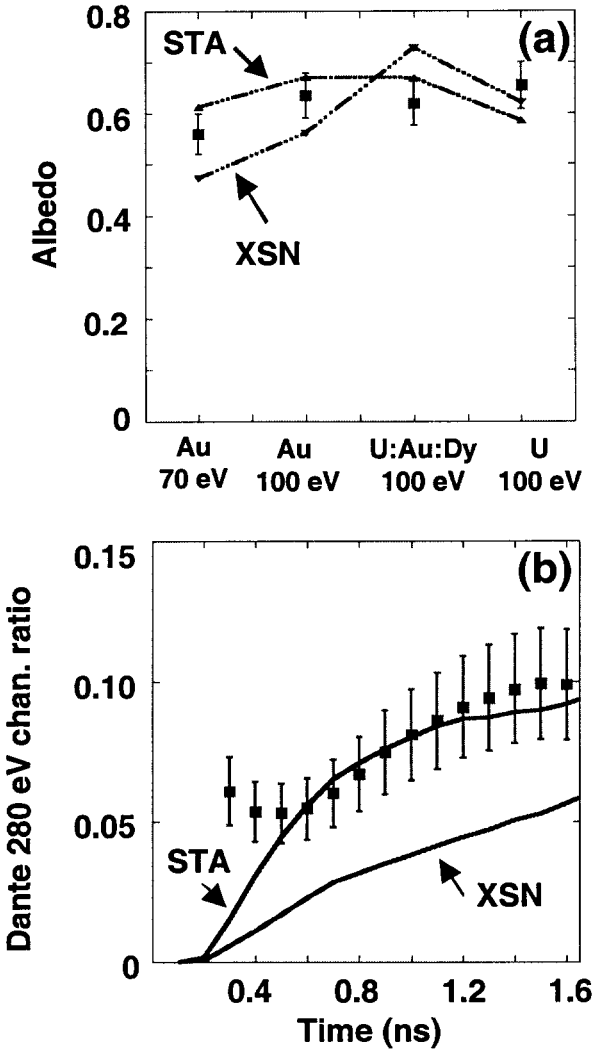
0.8
0.6
0.4
0.2
0
Albedo
STA
XSN
(a)
Au
70 eV
Au
100 eV
U:Au:Dy
100 eV
U
100 eV
0.15
0.10
0.05
0
Dante 280 eV chan. ratio
(b)
STA
XSN
0.4
0.8
1.2
1.6
Time (ns)

Fig. 4